

ASSESSMENT OF THE INTEGRITY OF DEGRADED STEAM GENERATOR TUBE BY THE USE OF HETEROGENEOUS FINITE ELEMENT METHOD

**Xinjian Duan, Michael Kozluk,
Atomic Energy of Canada Ltd.
Sandra Pagan,
Ontario Power Generation
Brian Mills,
Kinectrics Inc.**

1. INTRODUCTION

There is a need for *Fitness-For-Service Guidelines* (FFSG) for steam generator tubes used in the Canadian nuclear industry because a variety of degradations such as pitting, fretting wear, erosion-corrosion, thinning and denting have been observed and due to a unique set of tube size, tube support configurations, loading conditions and tube materials [1]. To assist with steam generator life cycle management, OPG has developed FFSG for steam generator tubes [2]. The FFSG are intended to provide standard acceptance criteria and evaluation procedures for assessing the condition of steam generator tubes for structural integrity, operational leak rate, and consequential leakage during an upset or abnormal event. Based on inspection results in conjunction with representative, postulated distributions of flaws in the un-inspected tubes, the FFSG provide an acceptable method of satisfying the intent of CSA-N285.4 and justifying the continued operation of degraded steam generator tubes.

Some non-mandatory empirical axial and circumferential flaw models are also provided in the FFSG for structural integrity assessments. The test data from the OPG Steam Generator Tube Testing Program (SGTTP) showed that the FFSG axial flaw model is conservative for a wide range of defect morphologies. A defect-specific axial flaw model was proposed for flat-bar fret defects in I800 tubes by utilizing the SGTTP database of extensive test results [3]. A defect-specific flaw model for outer diameter (OD) pitting and inner diameter (ID) inter-granular attack in Monel 400 tubes was also developed using the SGTTP test data. More tests have been scheduled to support the development of defect specific models for axial flaws (OD cracks or ID laps) in Monel 400 and to supplement the database for Monel 400 pits.

Predicting the remaining strength of degraded pipe/tube by the use of finite element methods has attracted great attention in recent years in both the petroleum and nuclear power industries to reduce the amount of expensive tests and to provide prompt assessment of emerging new degradation mechanisms. The key issue in the numerical analysis lies in which criterion is adopted to determine the failure load. The most commonly used methods are the twice-elastic slope and the tangent intersection method. Some work has indicated that these two approaches are too conservative and lack objectivity [4]. Some local approaches have also been proposed to check the local stress at the flawed region [5,6]. The deficiencies of the local criterion approach are that it is not applicable to defect-free tubes, and/or tubes with very high constraints/triaxiality, such as cracks.

Recently, a heterogeneous finite element model (HFEM) has been developed and successfully applied to predict the failure behaviour of ductile sheet metals under various deformation modes, i.e. plane stress, plane strain and 3-D [7]. A two-scale (micro-macro) model is applied to take

into account the heterogeneous microstructural distribution and the consequential scatter in the mechanical properties. These inhomogeneities are then explicitly incorporated into a large deformation finite element program. Material failure in the simulation arises naturally in the sequence of uniform deformation, diffuse necking, localized necking (micro-voids nucleation, growth and coalescence) and failure. Although strain increases dramatically after diffuse necking, the load changes little from diffuse necking to failure.

In this work, the HFEM is firstly validated by comparing the predicted failure modes and failure pressure with experimental observations for various tubes (defect-free, pits defect, uniform thinning, and axial slots). The HFEM is then applied to predict the failure pressure to be used in the Condition Monitoring Assessment of the removed steam generator tube R04C29 from the Picking Unit 1 Steam Generator 7. The Taguchi experimental design method is also applied to prioritize the flaw dimensions that affect the integrity of degraded steam generator tubes such as the defect length, depth, and width. An axial slot specific flaw model is finally presented to support a scheduled 2006 plant outage.

2. STEAM GENERATOR TUBE TESTING PROJECT

The Steam Generator Tube Testing Project (SGTTP) was initiated in April 1999 in response to two regulatory management actions [8]. Four types of tests have been performed on three different tubing materials (Monel 400, Inconel 600 and Incoloy 800) in the SGTTP: burst-pressure test, pressurized-bend test, leak-rate test, and material characterization test. The tested defects include pit(s), flat-bar fret, taper fork fret, axial/circumferential slot, circumferential thinning, and square defect etc., as shown in Figure 1. The geometry of defects was based on root cause assessments, metallurgical examinations of removed tubes, and ultrasonic testing scans of in-service tubes.

The present study focuses on the burst-pressure tests. These tests have been performed in the Burst-Test Facility at Kinectrics Inc., Toronto. The principal test result is the internal pressure at which the remaining defect ligament fails. A typical burst-pressure test involves heating the specimen to 288°C and then monotonically increasing the internal pressure of the test specimen. Quasi-static loading rates are used because they are considered to be conservative; as they result in the lowest values of measured burst-pressure. The test is over when the specimen fails.

3. HETEROGENEOUS FINITE ELEMENT METHOD

Most commercially produced alloys have inhomogeneities presenting at different length scales. Micro-scale and meso-scale refers to microstructure with a size less or greater than grain size, respectively. At the micro-length scale, the second phase particles are a major source of inhomogeneity. Figure 2 shows the microstructure of removed Monel 400 tubes from Pickering Unit 1. Using a micromechanical analysis, the influence of such local microstructure can be incorporated in the structural model. In other words, the stress-strain curves associated with inhomogeneities can be obtained from the micromechanical analyses using a series of unit cell models.

At the meso-scale, texture is a major source of inhomogeneity. The volume fraction of each component in an alloy can be easily measured using X-ray diffraction, neutron diffraction or

electron back scattered diffraction (EBSD). The strength difference between the regions with average behaviour that we call the “matrix” and the inhomogeneities can also be quantitatively calculated by the use of the Fourier transformation from measured EBSD data. In this work, we simplify the analysis and treat inhomogeneity phenomenologically by assigning regions that have a slightly higher or lower strength than the matrix. The “matrix” is assumed to have the average stress-strain response. The stress –strain curves for the “hard” and “soft” components are simply obtained by slightly shifting the stress-strain curve for the “matrix” up or down $\pm 3\%$. Thus the working hardening rate for all three phases are maintained the same.

The detailed application of the above micro-macro or meso-macro simulations has been reported in Reference [7].

A general-purpose three-dimensional finite element program, H3DMAP V7, is used to analyze the burst-pressure tests. The hybrid explicit dynamic relaxation solution is adopted to solve the incremental plasticity problems [9]. Two types of elements, 8-node brick element and 4-node tetrahedron element, are used. The von Mises yielding criterion is used.

Since the burst-pressure test stops only after the specimen fails, prediction of the fracture path is necessary in order to have a consistent comparison. The Rice and Tracey fracture criterion [10] is used to indicate the initiation of fracture. A physical separation of the specimen was not necessary in the simulation since the current focus is on the prediction of maximum failure pressure that occurs before failure.

The Rice and Tracey fracture criterion can be expressed as:

$$\int_0^{\bar{\epsilon}_f} \exp(1.5 \sigma_m / \bar{\sigma}) d\bar{\epsilon} = C \quad (1)$$

where $\bar{\epsilon}_f$ is the equivalent strain at fracture initiation, while σ_m and $\bar{\sigma}$ are the hydrostatic stress and the equivalent stress, respectively. C is failure parameter, to be determined by matching the predicted failure pressure with the measured failure pressure for a single case.

4. CALIBRATION OF FINITE ELEMENT MODEL

For the ductile metals used in the piping industry and nuclear steam generator tubing, substantial plastic deformation precedes failure in burst-pressure tests. The finite element analysis results of such a process are affected by many factors, i.e. the stress-strain relationship, element formulation, the type of element, mesh size, time step, convergence control, etc. Unlike elastic analysis, the refinement of mesh size in failure analysis does not lead to converged results. In other words, the smaller the mesh size, the greater strain (or failure parameter) is calculated. It is critical to conduct sensitivity study on these parameters, and to calibrate the finite element model to a known case before it is used to solve new/unknown problems.

4.1. Determination of Critical Failure Parameter

In the present work, the calibration of the finite element model is carried out by matching the predicted burst pressure with the measured value from the burst-pressure test of the tube with axial OD slot.

The simulated tube is 150-mm long. The OD and the thickness are 12.60 mm and 1.25 mm, respectively. The 25-mm slot is located in the specimen center. The depth of the slot is 75.03% through-wall. Both ends of the tube are constrained along the axial directions. A pressure ramp with a maximum of 40 MPa pressure is proportionally applied to the inside surface. The total number of elements is over 150,000. The recorded burst pressure for OD axial slot tube is 32.7 MPa.

Figure 3 shows the history of the failure parameter versus applied pressure. Three different kinds of time steps are adopted in the simulations. By matching the predicted failure pressure with the measured value, the critical failure parameters are determined to be 0.51, 0.87, 1.12 for the 5000, 20000 and 100000 time steps, respectively. These critical failure parameters will be used later to determine the failure pressure for the tube with other defects.

4.2. Validation of Finite Element Model

The SGTTP test results of the specimen with axial ID slot are used to validate the above failure criterion. The specimen has the ID of 12.59 mm and thickness of 1.25mm. The slot is 25-mm long and 75.43% through-wall deep.

Figure 4 presents the applied pressure-failure parameter curves for two simulations: one with 5000 time steps and another with 20000 time steps. Using the critical failure parameters in section 4.1, the failure pressure values were determined to be 33.0 MPa (5000 time steps) and 32.6 MPa (20000 time steps). The measured failure pressure for ID axial slot tube is 32.9 MPa. This indicates that we can use relatively small number of time steps and obtain the same accuracy as from a large number of time steps.

4.3. Mesh Size Effect

Figure 5 shows the mesh of a section in a 3D model containing an ID axial slot defect. The number of elements in the fine mesh model is twice that of the coarse mesh model in the flawed region.

The effect of mesh size on the predicted failure pressure is shown in Figure 6. The predicted failure pressure drops from 29 MPa to 28 MPa when the number of elements surrounding the defect doubles. The difference is less than 4%. To save computing time, a coarse mesh is used for other cases. It should be noted that the element size in the coarse mesh model is still less than 0.1 mm.

Figure 7 shows that necking precedes failure. There exists substantial plastic deformation in the flawed area. That is because Monel 400 and other steam generator tube alloys are very ductile.

4.4. Use of Tetrahedron Elements

Building a finite element model with pure brick (hexahedron) elements can be very challenging for some defects like pits and frets. Thus, it is necessary to evaluate the feasibility of using tetrahedron (tetra for short) elements. In this section, we first compare predictions between the use of brick and tetrahedron elements for a defect-free tube, and then simulate a tube with two pits and compare the predicted failure pressure with the measurements. It is also suggested that the proposed HFEM is further validated for different defects other than the ID axial slot defect.

Figure 8 shows the applied pressure – failure parameter curves for the use of brick and tetrahedron elements. A total amount of 100000 time steps were used in both simulations. The predicted failure pressure values are 102.5 MPa and 100.7 MPa for the use of brick (hexahedron) and tetrahedron (tetra for short) elements, respectively. The measured failure pressure varies from 99.2 MPa to 100.3 MPa. Also noticeable is the sharp increase of the failure parameter with a tiny increase in the applied pressure. In this case, as long as the critical failure parameter is greater than 0.5, the predicted failure pressure has little change. This phenomenon has also been observed in the simulations of other defects.

The mesh using tetrahedron elements of a Monel 400 tube with two identical pits (88.2% through-wall and 6.86 mm long) is shown in Figure 9. The calculated distribution of effective plastic strain is presented in Figure 10. The great similarity between the observed failure mode and the strain distribution confirms that the material experiences substantial plastic deformation before failure. In other words, the failure pressure is controlled by plastic collapse. Fracture mechanics is not applicable to these kinds of problems. The predicted failure pressure for this defect is 43.9 MPa, again very close to the measured value of 43.4 MPa.

It should be noted that a very fine mesh is required for the tetra elements to ensure the same high accuracy that the use of brick elements would give.

5. PREDICTING THE CHANGE OF FAILURE MODES IN CIRCUMFERENTIAL SLOTS

Understanding the change of failure modes with varied defect dimensions such as length is essential for the prediction of tube rupture. Figures 19 and 22 in Ref. [11] showed that the failure mode changes from circumferential rupture to axial leaking for uniform-thinning defects when the defect length increases from 4.8 mm to 38 mm. The same phenomenon was observed in the SGTTP for Monel 400 uniform thinning defects.

Figure 11 compares the distribution of effective plastic strain for two 360° uniform-thinning defects in Monel 400 with 5 mm and 20 mm length. Both defects are approximately 80% through-wall. The striking similarity between the strain distribution and the failure modes further supports the conclusion that the failure of Monel 400 under burst pressure test is by plastic collapse.

6. PREDICTION OF FAILURE PRESSURE OF A REMOVED TUBE

This section applies the knowledge obtained from the above sections to assess the removed Pickering Unit 1 Steam Generator 7 tube R04C29 (P1SG07R04C29). This tube was removed from the field for metallurgical examination because NDE detected a major flaw on the inner diameter surface. Laboratory ultrasonic (UT) and visual examinations measured the flaw length as 89-mm. The maximum depth of the flaw based on the metallurgical examination was 53% through-wall, including a sub-surface flaw. No burst-pressure test was carried out for this tube. Destructive metallurgical examination revealed the lap-type defect on the ID surface illustrated in Figure 12. The distances/depths 'a' and 'b' are 19% through-wall and 53% through-wall.

The defects in Figure 12 are characterized into two types of flaws for the numerical assessment. Flaw Type 1 includes a slot from the inside surface with depth 19%tw and a sub-surface lap with depth 53 %tw. Flaw Type 2 is a slot from the inside surface with total depth of 53%tw. The calculated distributions of effective plastic strain for both characterizations are compared in Figure 13. Completely different patterns of plastic strain are observed for the depth. Obvious necking is observed in the deep flaw (Flaw Type 2). The predicted failure pressure values are 68 MPa and 54.2 MPa for Flaw Type 1 and Flaw Type 2, respectively. The FFSG axial flaw model is not applicable to the characterization of Flaw Type 1 but is applicable to Flaw Type 2. The calculated failure pressure using the FFSG axial flaw model for Flaw Type 2 is 52 MPa. Therefore, based on the prediction of 54.2 MPa from the numerical assessment the FFSG axial flaw model is conservative for this kind of axial flaw.

The maximum normal operating pressure difference between the primary and second side of this tube in service was 8.7 MPa which occurs during a small temporal window at startup and shutdown. The maximum pressure differential for accident or faulted conditions is 9.5 MPa during a main steam line break. Therefore based on the predicted failure pressures from the numerical assessment the factors of safety during normal operation are approximately 8 and 6 for Flaw Types 1 and 2, respectively. These factors of safety are greater than those required by the Prohibiting Leakage Acceptance Criteria of the FFSG. Therefore, this tube passes the Condition Monitoring Assessment.

7. PARAMETER SENSITIVITY STUDY

A sensitivity study was also carried out to assess the effect of the flaw dimensions on the predicted failure pressure, by the Taguchi method. The Taguchi method adopts a set of standard orthogonal arrays (OA) to determine the configuration of parameters and to analyse the results. The arrays use a small number of experimental runs to obtain maximum information with high reproducibility and reliability.

Three general adjustable parameters were utilized: flaw length, width, and depth. Each of the parameters was assigned three values (also called 'levels'). These values are shown in Table 1. All these values were selected based on the lab examination of the removed tube from Pickering Unit 1. The value of flaw length ranges from 25 mm to 75 mm. The flaw width increases from 0.25 mm to 1 mm. The depth ranges from 40% to 80%. For volumetric examination, the CSA standard CAN/CSA-N285.4-94 requires "the predicted wall loss will not exceed 40% of the nominal wall thickness prior to the next inspection". A fitness-for-service assessment must be

submitted to the regulatory authority for indications that are left in-service and that do not comply with this acceptance criterion. Therefore, the flaw depth is selected beyond 40% through-wall. The designed orthogonal array, L9(3³), is shown in Table 2. Designation L9(3³) indicates that there are three parameters, each parameter has three levels and total nine test runs need to be conducted.

The relative contribution of each parameter towards the failure pressure is analyzed via the analysis of variance (ANOVA) method. ANOVA uses the sum of squares to quantitatively examine the deviation of the responses of each control factor from the overall experimental mean response. The calculated contributions of each parameter to the failure pressure are 0.9%, 1.6% and 97.1% for flaw length, width and depth. Hence, flaw depth is the most important parameter controlling the failure pressure. The contributions of width and length are insignificant. This is understandable because the minimum flaw length (25 mm) is twice of the tube diameter (12.6 mm). If the flaw length is reduced below the tube radius of 6.3 mm, the impact of flaw length on failure pressure would be significant, as illustrated Section 5. However, the flaw depth is still the dominating parameter of the burst-pressure.

The average effect of each parameter level on the failure pressure is shown in Figure 14. It can be seen that the failure pressure drops almost linearly with increasing flaw depth between 40% to 80% of tube wall.

8. DEVELOPMENT OF AXIAL SLOT SPECIFIC FLAW MODEL

To demonstrate increased margins of safety of the FFSG axial flaw model to the axial slot defect, an ID/OD axial slot specific flaw model for Monel 400 is developed here. Figure 14 shows that failure pressure drops almost linearly with increasing flaw depth. Therefore, the power of the term of a/t is selected to be 1, where a is the flaw depth and t is the wall thickness at flawed area. For the axial defect, the circumferential hoop stress is the parameter that controls the failure.

For defect-free tube/piping, the following relationship stands between the hoop stress σ_{Hoop} and the applied pressure P :

$$\sigma_{Hoop} = P \frac{D_i}{2t} \quad (2)$$

where D_i is the inside diameter. The failure pressure of the degraded P_{pred} is expressed in a simple form of

$$P_{pred} = P' \left(1 - A \frac{a}{t}\right) \quad (3)$$

where P' is the failure pressure of the defect-free tube, A is a variable to reflect the contribution from the flaw width and depth. Considering the difficulty of acquiring the information of flaw width from the NDE, A is assumed to be a function of only flaw length.

By regressing the SGTTP test results for six OD and ID axial slots in Monel 400 and the FE predictions, the final form of the new axial slot specific flaw model takes in the following format,

$$P_{pred} = \sigma_M \frac{2t}{D_i} \left[1 - \frac{a}{t} \left(1 - \exp \left(-0.103 \frac{L}{\sqrt{R_i(t-a)}} \right) \right) \right] \quad (4)$$

where σ_M is a material parameter. σ_M equals 407 MPa for Monel 400. This value was obtained by matching the predicted failure pressure with the measured failure pressure of defect free tube. R_i is the inside radius at the flawed region, and L is the flaw length.

Additional burst tests on Monel 400 axial slots are in progress under the OPG's SGTTP and will be used to validate/refine the new axial slot model.

9. CONCLUSIONS

Although not discussed in this paper, the present methodology has also been applied to assess the structural integrity of large diameter piping. The following conclusions are drawn from this study:

- ❖ The heterogeneous finite element method is an effective approach for determining the remaining steam generator tube strength. It not only calculates the correct failure pressure for a variety of defects, but also predicts the correct change of failure mode.
- ❖ The flaw depth is the dominant parameter controlling the failure pressure. The failure pressure varies almost linearly with defect depth when the defect length is greater than 2 times tube diameter.
- ❖ The removed tube P1SG07R04C29 passed the Condition Monitoring Assessment according to the requirements of the FFSG.
- ❖ Axial slot specific flaw model has been developed for Monel 400 based on the hybrid database.

10. ACKNOWLEDGEMENTS

The authors thank Drs. Don R. Metzger, Wolf Reinhardt, Richard Savu , Siavash Khajehpour for many helpful discussions and the review of this work.

11. REFERENCES

- [1] R.L. Tapping, J. Nickerson, P. Spekkens, C. Maruska, CANDU Steam Generator Life Management, Nuclear Engineering and Design, 2000, Vol.197, pp.213-223.

- [2] S. Pagan, D. Scarth, Fitness-for Service Guidelines for Steam Generator Tubes, Section 1: Evaluation Procedures and Acceptance Criteria, Ontario Power Generation report N-REP-33110-10000-R001, 2005 October 4.
- [3] S. Pagan, B. Mills, M. Kozluk, Fitness-for-Service Assessment for Steam Generator Tube Fretting at Darlington Nuclear Generating Station, 2006 Pressure Vessels & Piping Conference and the Eleventh International Conference on Pressure Technology, Paper Number PVP2006-ICPVT11-93787, 2006 July 23-27, Vancouver, British Columbia, Canada.
- [4] H. Li, D. Mackenzie, Plastic Collapse Analysis of Pipe Bends under Out-of-Plane Moment and Internal Pressure Loading, 2006 Pressure Vessels & Piping Conference and the Eleventh International Conference on Pressure Technology, Paper Number PVP2006-ICPVT11-93098, 2006 July 23-27, Vancouver, British Columbia, Canada
- [5] D.J. Shim, J.B. Choi, Y.J. Kim, Failure Strength Assessment of Pipes with Local Wall Thinning under Combined Loading Based on Finite Element Analyses, Journal of Pressure Vessel Technology, Transactions of the ASME, 2004, Vol. 126, pp.179-183.
- [6] D.S. Cronin, R.J. Pick, Prediction of the Failure Pressure for Complex Corrosion Defects, International Journal of Pressure Vessels and Piping, 2002, Vol. 79, 279-287.
- [7] X. Duan, M. Jain, D.S. Wilkinson, Development of A Heterogeneous Microstructurally Based Finite Element Model for the Prediction of Forming Limit Diagram for Sheet Material, Metallurgical and Materials Transactions A, 2006 (In Press).
- [8] M.J. Kozluk, D.G. Martin, B.E. Mills, Ontario Power Generation's Steam Generator Tube Testing Project, Proceedings of the CNS 4th International Steam Generator and Heat Exchanger Conference, Toronto, 2002 May.
- [9] R.G. Sauvé, D.R. Metzger, A Hybrid Explicit Solution Technique for Quasi-Static Transients, Proceedings of the 1996 ASME Pressure Vessels and Piping Conference, 1996, Vol. 326, pp. 151-157.
- [10] J.R. Rice, D.M. Tracey, On Ductile Enlargement of Voids in Triaxial Stress Fields, Journal of the Mechanics Physics of Solids, 1969, vol. 17, pp. 201-217.
- [11] J.M. Alzheimer, R.A. Clark, C.J. Morris, M. Vagins, Steam Generator Tube Integrity Program Phase I Report, U.S. Nuclear Regulatory Commission, NUREG/CR-0718, 1979 September.

Table 1: Flaw Dimensions used in the Taguchi Robust Design

All parameters were selected based on the metallurgical examinations of the removed tubes from Pickering Units 1 to 4.

Variable	Level 1	Level 2	Level 3
Length	25 mm	50 mm	75 mm
Width	0.25 mm	0.5 mm	1.0 mm
Depth	40%	60%	80%

Table 2: Taguchi Robust Design and the Failure Pressure

Simulation No.	Length	Width	Depth	Failure Pressure
1	25 mm	0.25 mm	40%	61.7 MPa
2	25 mm	0.50 mm	60%	48.9 MPa
3	25 mm	1.0 mm	80%	29.2 MPa
4	50 mm	0.25 mm	60%	43.7 MPa
5	50 mm	0.50 mm	80%	23.9 MPa
6	50 mm	1.0 mm	40%	67.4 MPa
7	75 mm	0.25 mm	80%	23.4 MPa
8	75 mm	0.50 mm	40%	64.3 MPa
9	75 mm	1.0 mm	60%	46.3 MPa

Figure 1. Tube Configurations

The geometries for the flaws were chosen as conservative characterizations of generic degradation that had been observed. The test matrix included specimens without flaws.

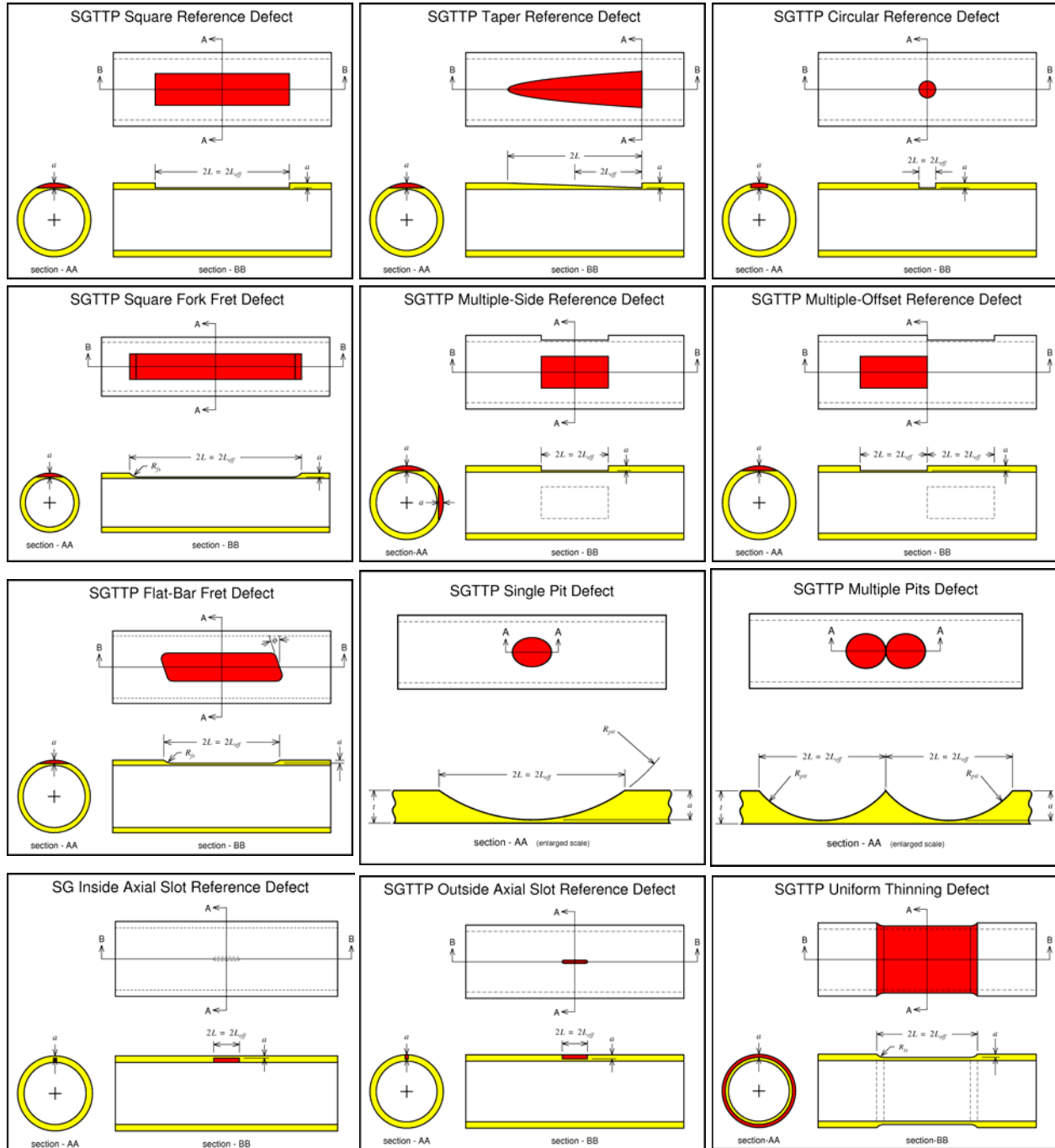


Figure 2. Microstructure in Removed Monel 400 Tubes

Texture and particle distribution in the removed steam generator Monel 400 tubes from Pickering Unit 1 SG6. The material is heterogeneous.

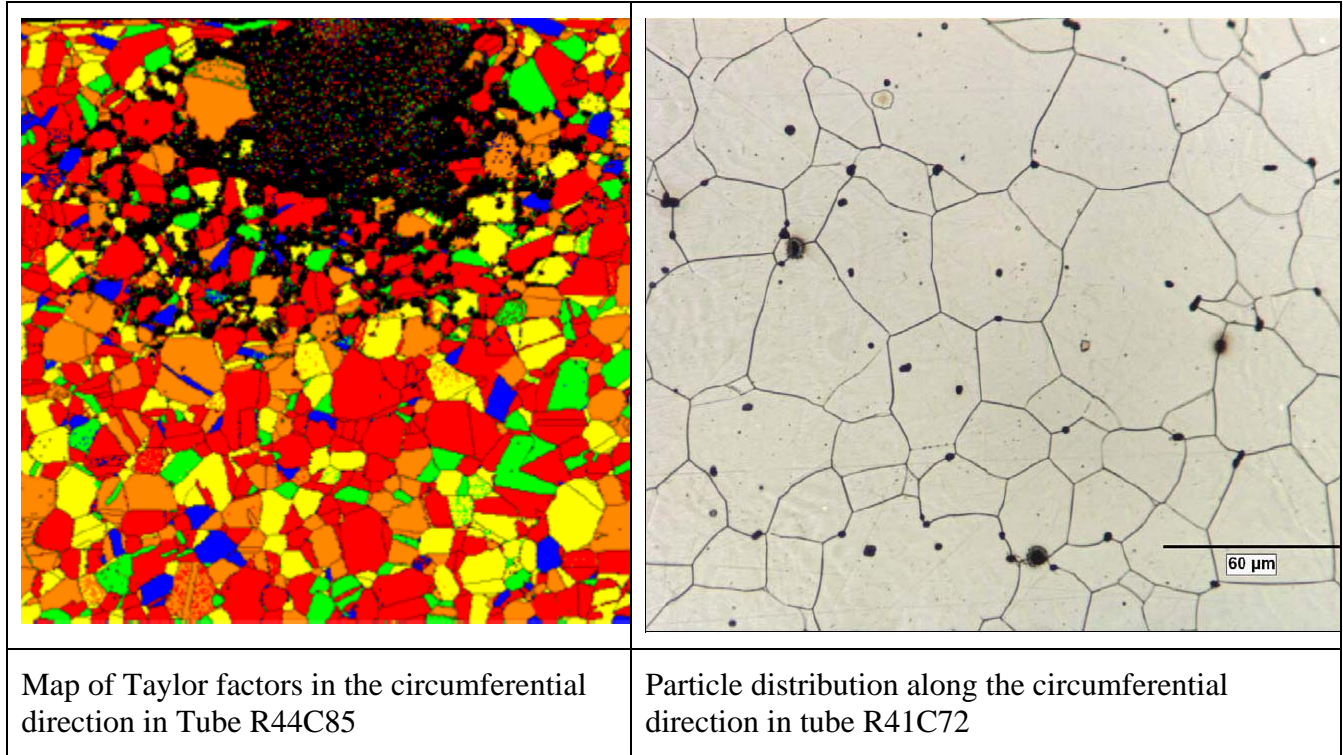


Figure 3 Determination of the Critical Failure Parameter

The burst-pressure test of the tube with OD axial slot is used to calibrate the failure criterion and the mesh size. The measured failure pressure is 32.7 MPa. The critical failure parameters increase with increasing number of time steps. The critical failure parameters are 0.51, 0.87, and 1.12 for the 5000, 20000, and 100000 time steps, respectively.

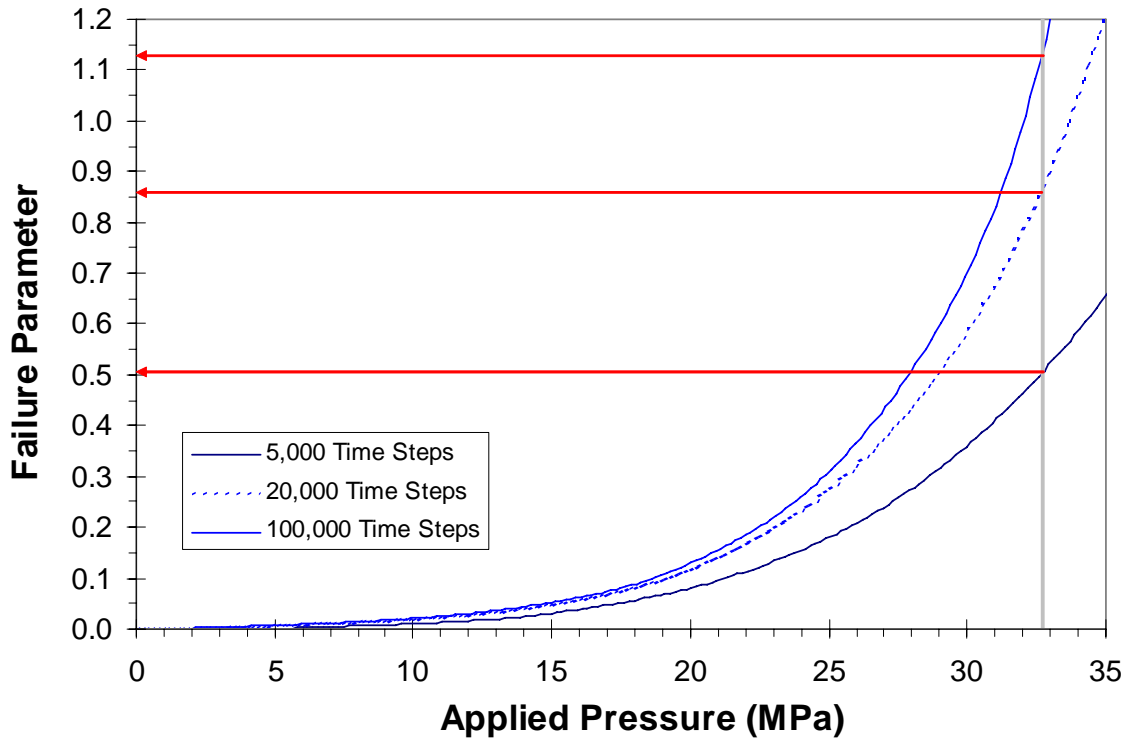


Figure 4 Prediction of the Failure Pressure for Tube with ID axial slot

This case is used to validate the finite element model and the failure criterion for the tube with ID axial slot. The predicted failure pressure values are 33. MPa and 32.6 MPa for the use of 5000 time steps and 20000 time steps. The measured failure pressure is 32.9 MPa. Obviously, an excellent agreement was given.

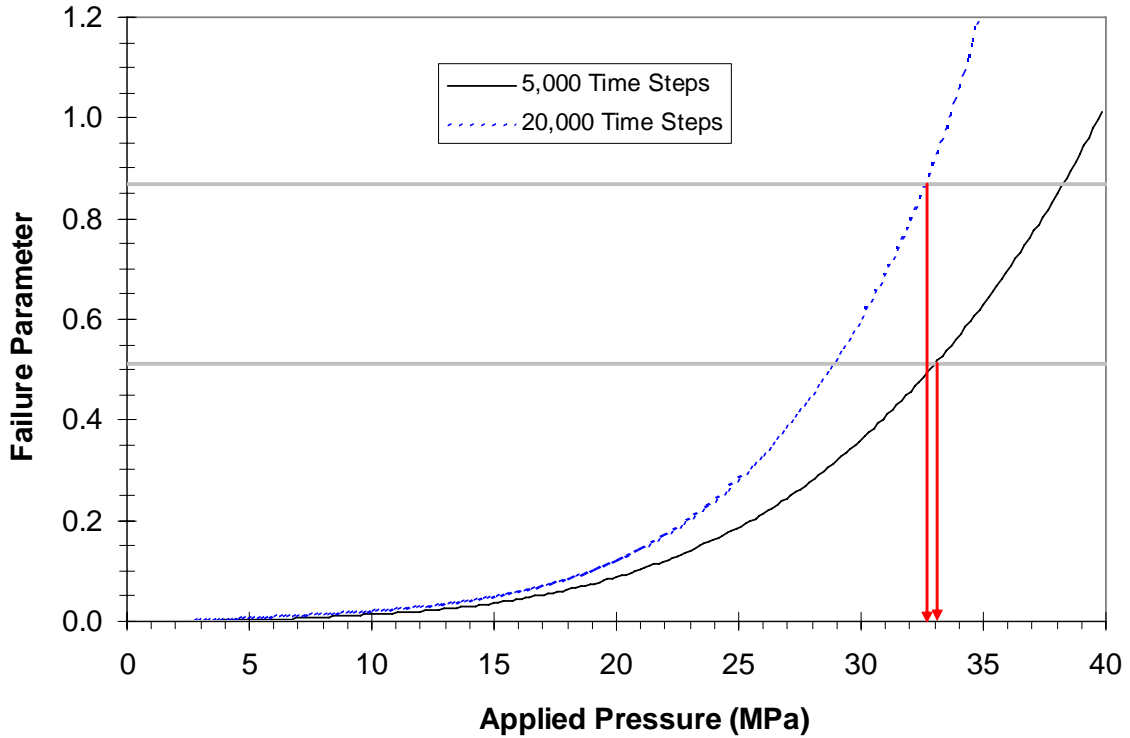


Figure 5. Finite Element Mesh

The number of elements around the bottom of the slot in the fine mesh model is 2 times of the elements in the coarse mesh model.

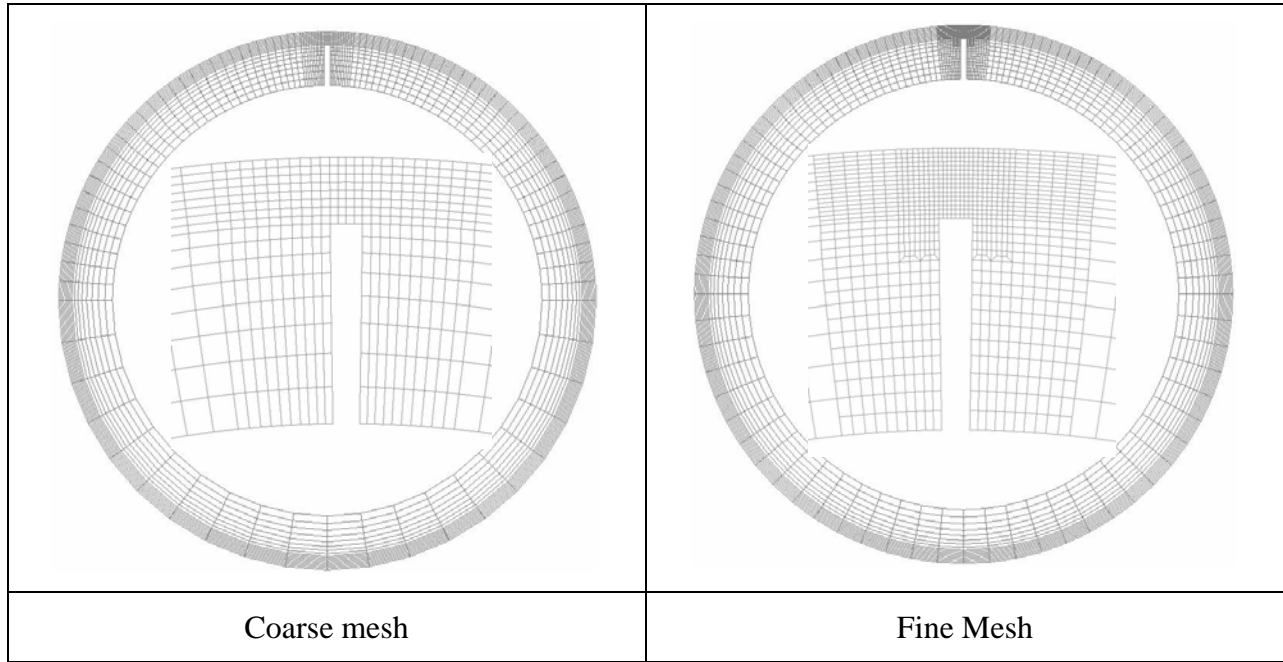


Figure 6. Effect of Mesh Size on the Failure Pressure

The predicted failure pressure values are 29 MPa and 28 MPa for the coarse and fine mesh model. The difference is less than 4%. A total amount of 100,000 time steps were used. The critical failure parameter is 1.12.

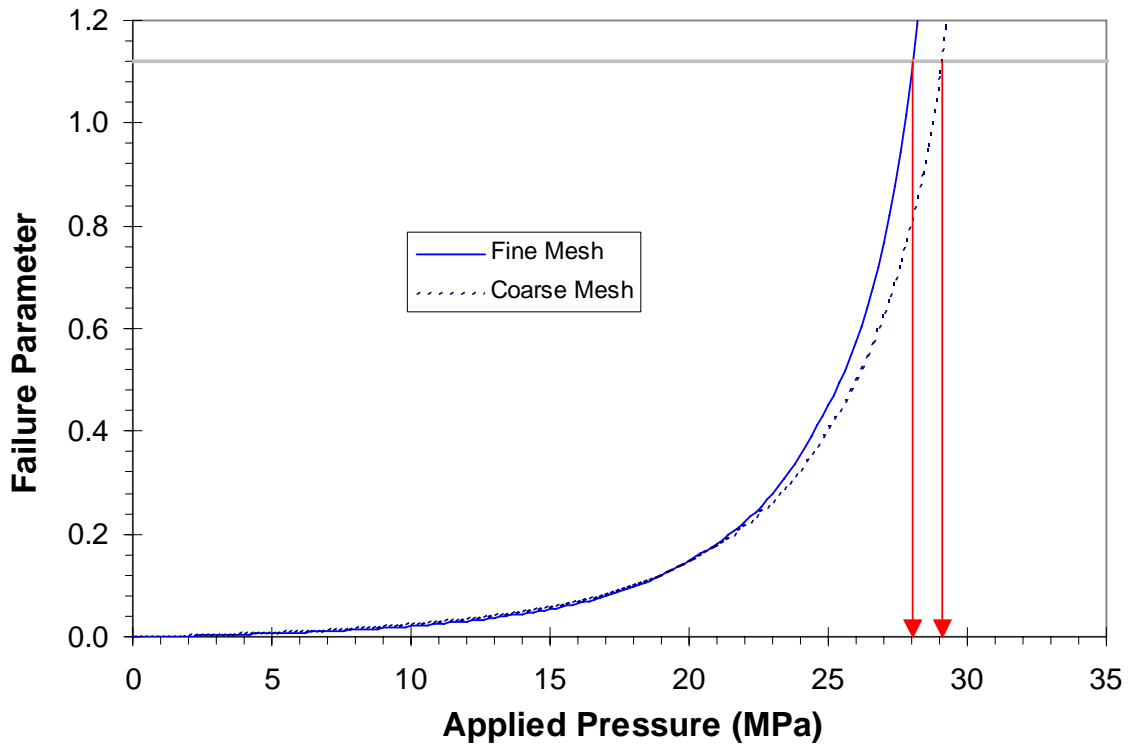


Figure 7. Distribution of Effective Plastic Strain At Failure

Obvious necking phenomenon for both cases.

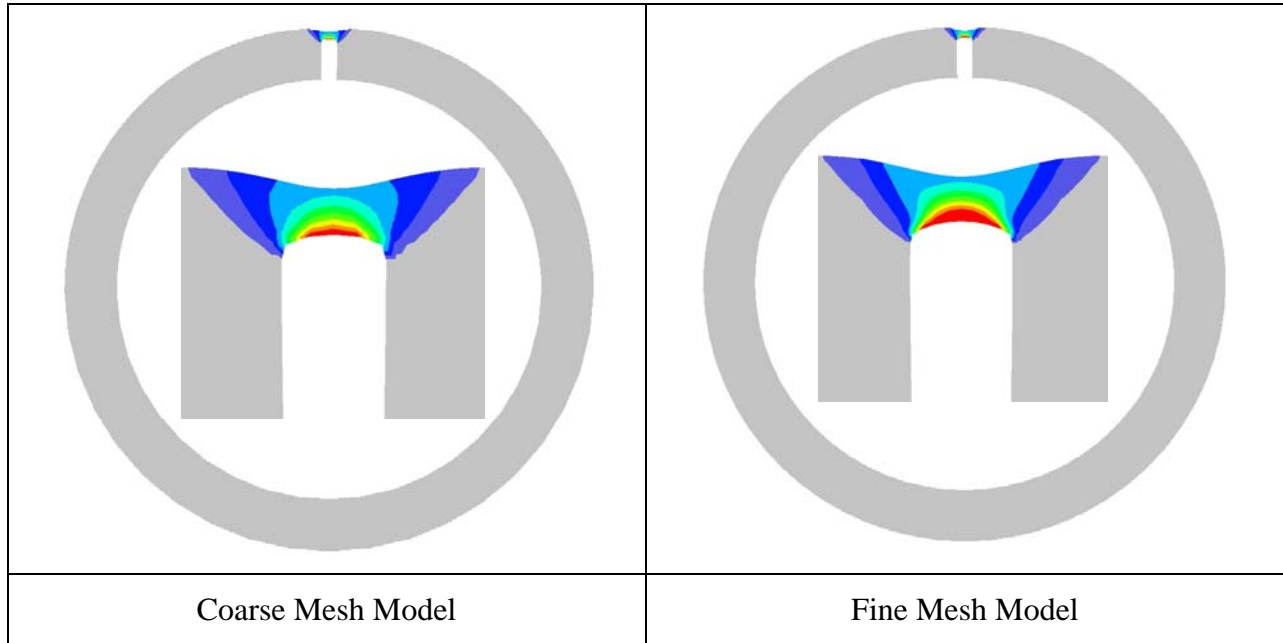


Figure 8. Comparison between Brick and Tetra Elements for Defect-Free Tube

A total amount of 100000 time steps were used in both simulations. The predicted failure pressure values are 102.5 MPa and 100.7 MPa for the use of brick (hexahedron) and hexahedron (tetra for short) elements, respectively. The measured failure pressure varies from 99.2 MPa to 100.3 MPa. Also noticeable is the sharp increase of the failure parameter with a tiny increase in the applied pressure. In this case, as long as the critical failure parameter is greater than 0.5, the predicted failure pressure has little change. This phenomenon has also been observed in the simulations of other defects.

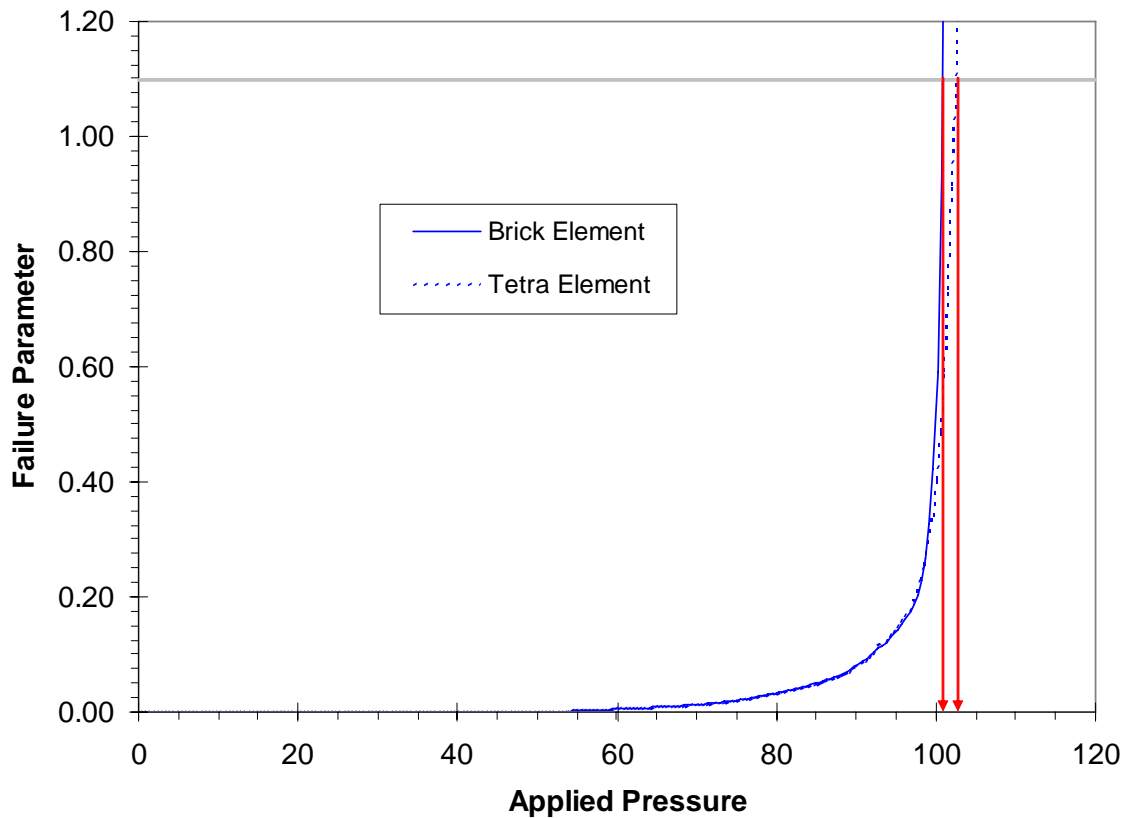


Figure 9 Finite Element Mesh of Two 88 or 89 %tw Pit Flaws

Mesh with tetra elements would reduce the pre-processing time in a factor of 10. Over 350,000 elements were used in the simulation. Each pit is approximately 6.85 mm long and 88% through-wall. The predicted and measured failure pressure values are 45.1 MPa and 43.4 MPa.

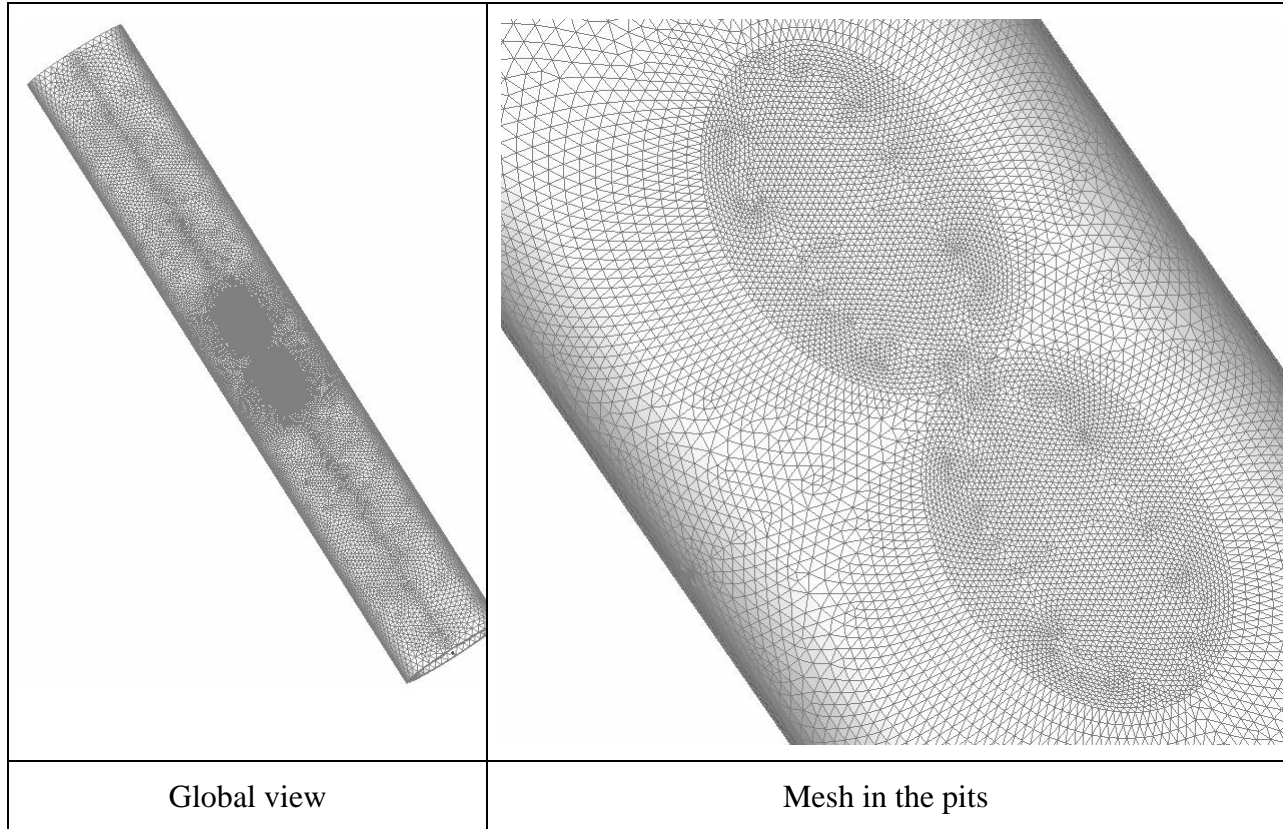


Figure 10. Distribution of the Effective Plastic Strain and the Observed Failure mode

Both pits were approximately 88% through-wall deep. Tetra elements were used.

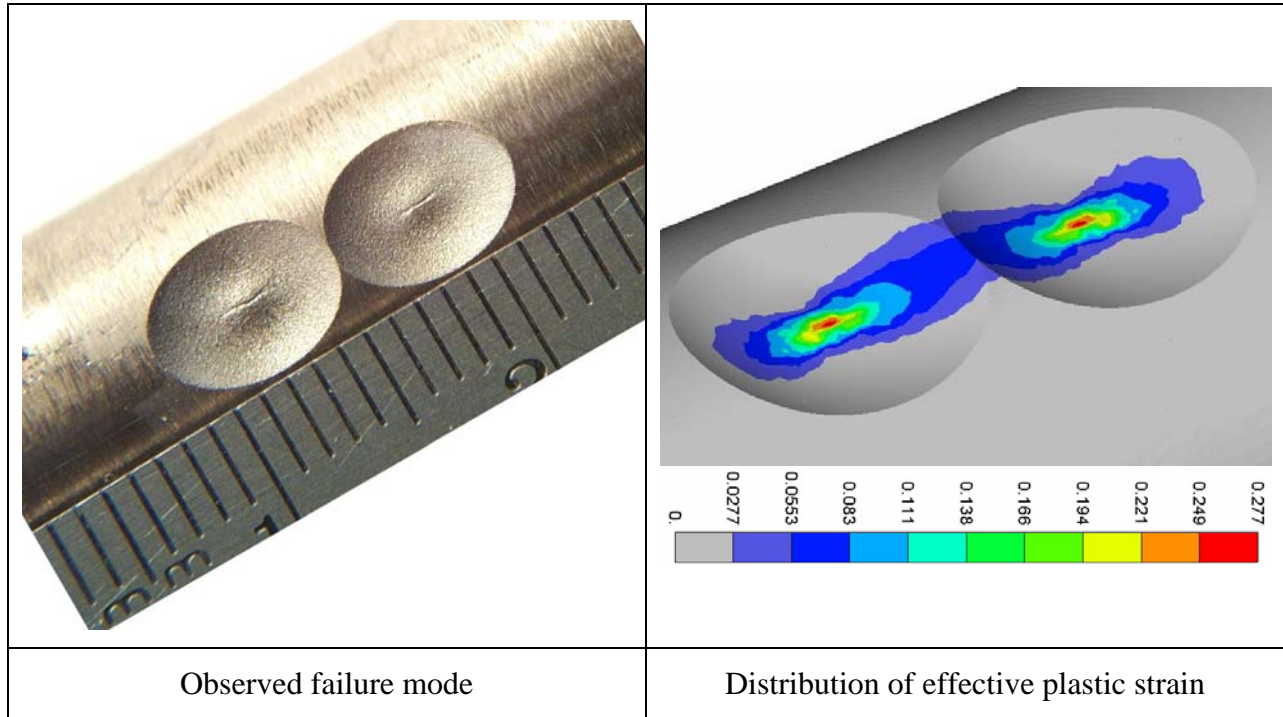


Figure 11. Change of Failure Modes

The lengths are 3 mm and 20 mm for the longer and shorter flaws in the simulations. The experimental observations were taken from Ref.[13].

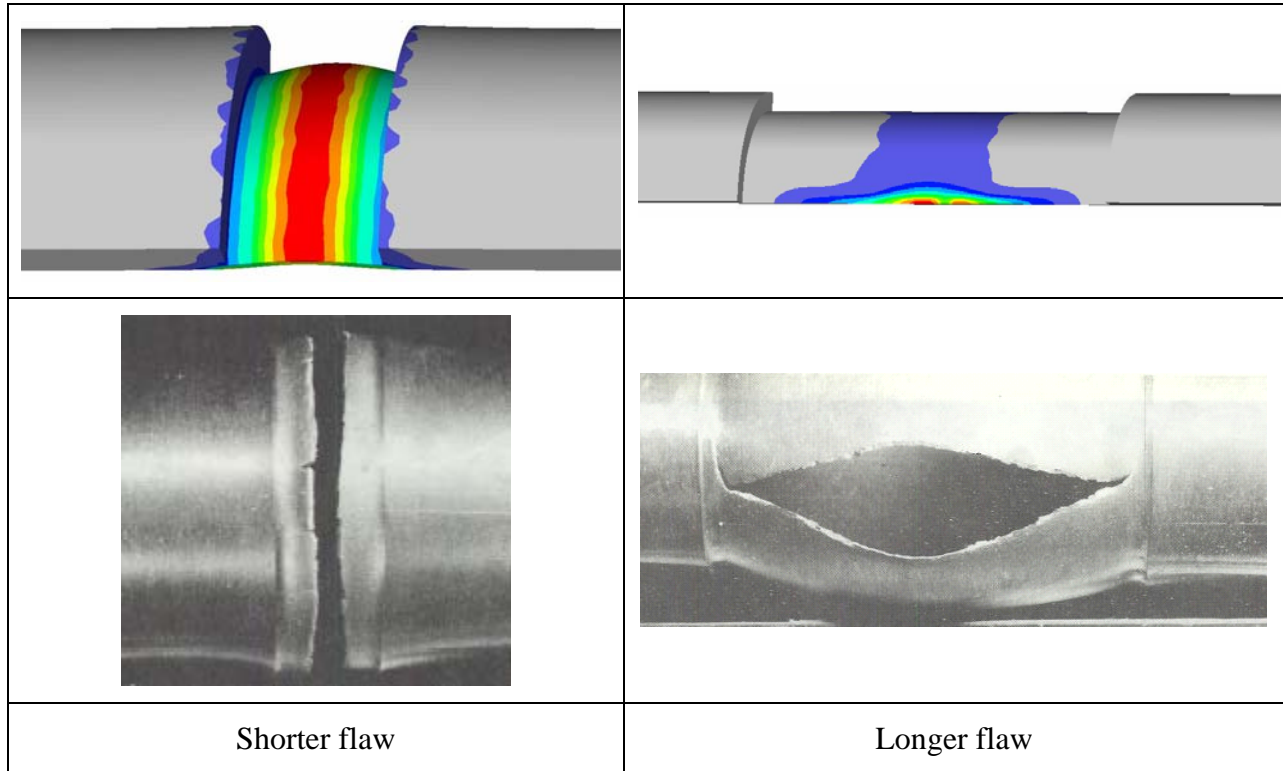


Figure 13. Flaw Characterization and Distribution of Effective Plastic Strain

This is a cross section of a removed tube from Pickering Unit 1. Two kinds of flaw are characterized. The distance 'a' and 'b' are 19% and 53% through-wall. The predicted failure pressure values are 68 MPa and 54.2 MPa for Flaw Type 1 and Flaw Type 2, respectively.

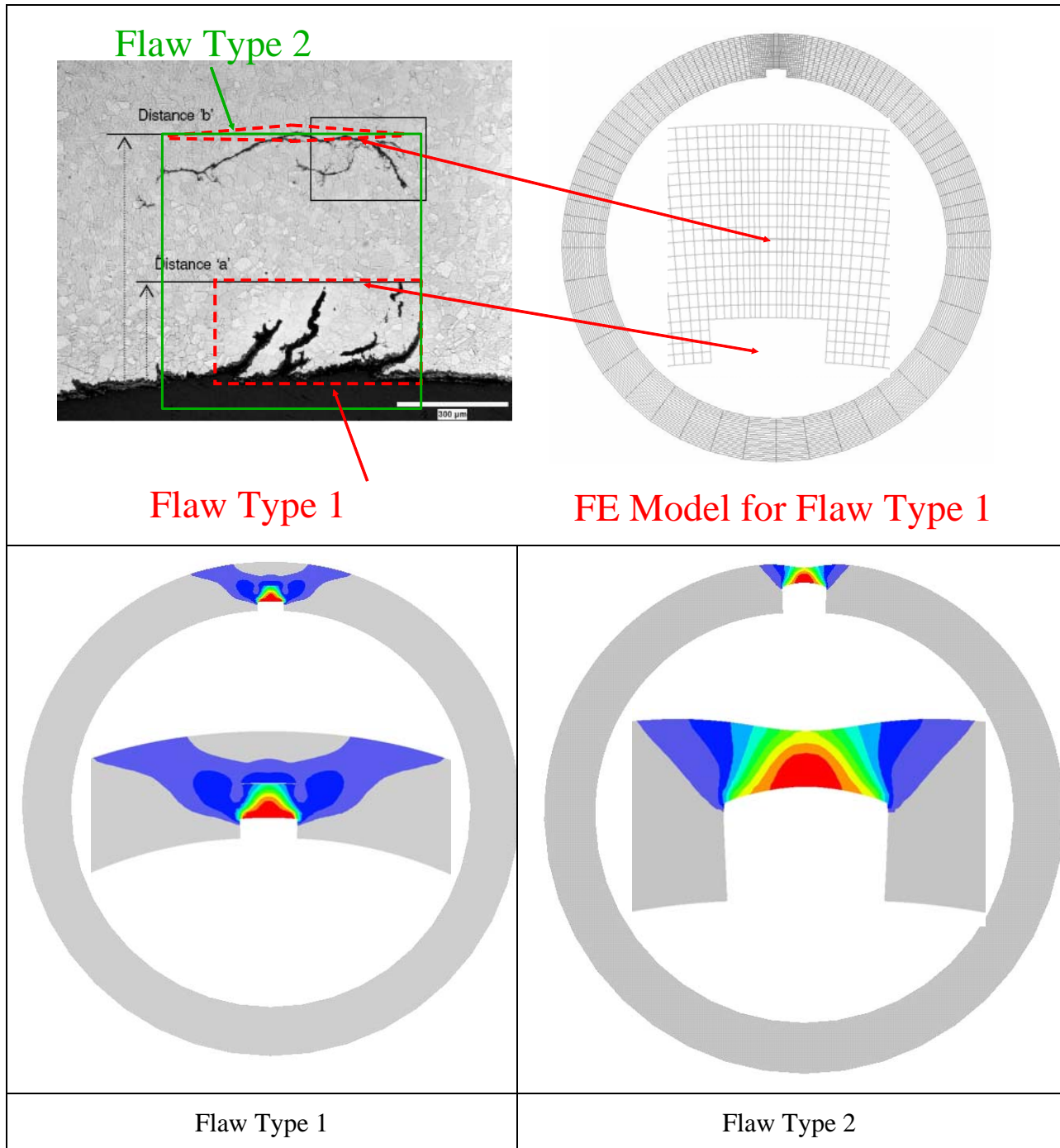


Figure 14 Variation of Failure Pressure with Flaw Dimensions

